XXXVI Ibero-Latin American Congress on Computational Methods in Engineering
CILAMCE
Rio de Janeiro, 22-25 Nov 2015

CO-SIMULATION FOR VIV ANALYSIS USING IMMERSED BOUNDARIES AND GEOMETRICALLY-EXACT BEAM THEORIES WITH CONTACT

Luiz Felipe Marchetti do Couto

luiz.couto@usp.br

Henrique Campelo Gomes

henrique.campelo@usp.br

Departament of Structural and Geotechnical Engineering, Polytechnic School at University of São Paulo

Av. Prof. Almeida Prado, travessa 2, 83, Cidade Universitária, São Paulo, SP, 05508-900, Brazil

Alfredo Gay Neto

alfredo.gay@usp.br

Departament of Structural and Geotechnical Engineering, Polytechnic School at University of São Paulo

Av. Prof. Almeida Prado, travessa 2, 83, Cidade Universitária, São Paulo, SP, 05508-900, Brazil

Paulo de Mattos Pimenta

ppimenta@usp.br

Departament of Structural and Geotechnical Engineering, Polytechnic School at University of São Paulo

Av. Prof. Almeida Prado, travessa 2, 83, Cidade Universitária, São Paulo, SP, 05508-900, Brazil

Abstract. *This work deals with a class of fluid-structure interaction problems in which the structure can move with large displacements including contact interaction with other bodies or itself. The structure is modeled using geometrically-exact rods, including the possibility of contact interaction with rigid walls representing the boundary of the desired physical domain. Furthermore, self-contact searching is also addressed for particular situations when the structure tries to touch itself. Both contact with the walls and self-contact consider large displacements possibility, including normal and friction effects using a penalty approach. The* *interaction between fluid and structure domains is solved by an immersed boundary approach that uses discontinuous Lagrange multipliers to enforce kinematic and force equilibrium along the interface between the non-matching overlapping meshes, in an alternative to usual Arbitrary Lagrangian Eulerian (ALE) approaches. The engineering applicability of the proposed work is of great interest to deep water offshore oil exploitation. Risers structures usually are subjected to sea current effects and many important phenomena such as vortex induced vibration (VIV) is a result of fluid-structure interaction. The proposed technique uses few degrees of freedom to solve the structural problem, since structural rod elements are considered. Bi-dimensional unsteady flow of an incompressible viscous fluid is adopted, and the interaction with the structural model is enforced by a separate solution of structure and fluid problems, connected by loading and displacements updating during simulation, step by step, along a dynamic transient time evolution.*

Keywords: *Fluid-Structure Interaction, Immersed Boundaries, Geometrically-Exact Beam Theory, Contact*

1 INTRODUCTION

Fluid-Structure Interaction has become an important and successful method of computational simulation that involves the interaction between fluid and structural dynamics (Gomes, 2013). The main reason is that most of the engineering applications involve some sort of FSI problem and algorithms and successfully model various applications ranging from Civil Engineering to Geophysical, Aerodynamical and also Offshore structures.

Some of the challenges that numerical modeling of FSI offers are, among others, the spatial domain occupied by the fluid changes in time as the interface moves and the mathematical model to handle that. Accurate representation of the flow field near the fluid-structure interface requires that the mesh be updated to track the interface and this requires special attention in 3D problems with complex geometries (Tezduyar, 2005).

In this work, interaction between an incompressible fluid flow at low Reynolds number and an offshore structure ("riser") that we could consider as a flexible circular cylinder, in two dimensions has been studied. The global analysis of risers is important during design of an offshore production plant and nonlinear static analyses are commonly performed, considering hydrodynamic loadings from currents. And also, the dynamic analysis should be performed since it could affect riser fatigue life (Gay Neto et al., 2015). A geometrically-exact beam theory with seabed contact was used in this work.

One of the difficulties in simulating FSI with risers is the sea current speed and the fluid properties (e.g. density and viscosity) which normally leads to high Reynolds number. This effects require some sort of numerical stabilization (convective dominated flow) (Elias et al., 2009, Forster et al., 2007) and complex turubulence models. Add the fact that the model and simulation, in general, require a large number of elements (Finite Element fluid meshes) and resonably extent in time range in order to identify some effects (e.g. VIV, flutter).

This work is divided in three main sections. The first section will cover the FSI with Immersed Boundary method theory. The second section will handle the contact and structural models of risers. The last main section will discuss the methodology of analysis of a staggered scheme using two different in-house solvers, HPC LMC and GIRAFFE, both developed in C++. This section will also cover a numerical simulation of the interaction between the fluid and the riser, starting with the analytical solution of an ellipse (result of section cut between an horizontal plane and the riser), following a steady state problem, to test the theory and methodology of analysis and the analytical solution of the ellipse, and finally the results of an unsteady state problem.

2 FLUID-STRUCTURE INTERACTION

2.1 Navier Stokes equations

Let Ω_t in $\mathbb{R}^{n_{sd}}$ be the spatial domain with boundary Γ_t at time $t \in (0, T)$. The subscript t indicates the time-dependence of the domain. The Navier-Stokes equations of incompressible flows are written on Ω and $\forall t \in (0, T)$ as

$$\rho \left(\frac{\partial \boldsymbol{u}}{\partial t} + \boldsymbol{u} \cdot \nabla \boldsymbol{u} \right) \;=\; \nabla \cdot \boldsymbol{T} + \rho \boldsymbol{b}, \tag{1}$$

$$\nabla \cdot \boldsymbol{u} \;=\; 0, \tag{2}$$

where ρ, $\boldsymbol{u}$ and $\boldsymbol{b}$ are the density, velocity and the external force vector, respectively. For a Newtonian fluid the stress $\boldsymbol{T}$ and the strain rate tensors $\epsilon\left(\boldsymbol{u}\right)$ are defined as

$$\boldsymbol{T} \;=\; -p\boldsymbol{I} + 2\mu\boldsymbol{\epsilon}\left(\boldsymbol{u}\right) \tag{3}$$

$$\boldsymbol{\epsilon}\left(\boldsymbol{u}\right) \;=\; \frac{1}{2}\left[\nabla\boldsymbol{u} + \left(\nabla\boldsymbol{u}\right)^{\mathsf{T}}\right] \tag{4}$$

Here p is the pressure, $\boldsymbol{I}$ is the identity tensor, μ is the viscosity.

The divergence of the stress tensor is written as

$$\nabla \cdot \boldsymbol{T} = -\nabla p + \mu\nabla^2\boldsymbol{u} + \mu\nabla(\nabla \cdot \boldsymbol{u}) \tag{5}$$

Since it is assumed that the flow is incompressible, the last term is zero. Therefore

$$\frac{\partial \boldsymbol{u}}{\partial t} + \boldsymbol{u} \cdot \nabla\boldsymbol{u} = -\nabla p + \nu\nabla^2\boldsymbol{u} + \boldsymbol{b}. \tag{6}$$

Note that all terms are divided by ρ in Eq. 6, originating the fluid kinematic viscosity ν and the kinematic pressure p.

2.2 Boundary and initial conditions

The essential and natural boundary conditions for Eq. (1) are represented as

$$\boldsymbol{u} = \overline{\boldsymbol{u}} \quad \text{on} \quad \Gamma_u, \tag{7}$$

$$\left(\nu\nabla\boldsymbol{u} - p\boldsymbol{I}\right)\boldsymbol{n} = \bar{\boldsymbol{t}} \quad \text{on} \quad \Gamma_t, \tag{8}$$

$$\boldsymbol{u} = \boldsymbol{u}_0 \quad \text{on} \quad \Omega \;\; \text{and} \;\; t = 0. \tag{9}$$

2.3 Weak form

Choosing arbitrary functions $\boldsymbol{w} \in \mathcal{H}_0^1\left(\Omega\right)$ and $q \in \mathcal{L}_2\left(\Omega\right)$ for the velocities and pressure test functions respectively, we can write the system of partial differential equations described by Eq. (6) in the equivalent integral form as

$$\left(\boldsymbol{w}, \dot{\boldsymbol{u}}\right)_\Omega + \left(\boldsymbol{w}, \boldsymbol{u} \cdot \nabla\boldsymbol{u}\right)_\Omega = -\left(\boldsymbol{w}, \nabla p\right)_\Omega + \left(\boldsymbol{w}, \nabla \cdot \left(2\nu\nabla^s\boldsymbol{u}\right)\right)_\Omega - \left(q, \nabla \cdot \mathbf{u}\right)_\Omega + \left(\boldsymbol{w}, \boldsymbol{b}\right)_\Omega \tag{10}$$

$\forall\left(\boldsymbol{w}, q\right)$. Now, integrating by parts the viscous and pressure terms, the weak form of the Navier-Stokes equation for incompressible fluid flow problems can be defined as

$$\left(\boldsymbol{w}, \dot{\boldsymbol{u}}\right)_\Omega + c\left(\boldsymbol{u}; \boldsymbol{w}, \boldsymbol{u}\right)_\Omega = -\left(p, \nabla \cdot \boldsymbol{w}\right)_\Omega - a\left(\boldsymbol{w}, \boldsymbol{u}\right)_\Omega - \left(q, \nabla \cdot \boldsymbol{u}\right)_\Omega - \left(\boldsymbol{w}, \bar{\boldsymbol{t}}\right)_{\Gamma_t} + \left(\boldsymbol{w}, \boldsymbol{b}\right)_\Omega \tag{11}$$

$\forall\left(\boldsymbol{w}, q\right)$. Note that the boundary term over Γ vanishes at Γ_u because of the test function. The convective and viscous terms have been written in a compact notation defined by the following bilinear and trilinear forms:

$$a\left(\boldsymbol{w}, \boldsymbol{u}\right)_\Omega \;=\; \int_\Omega \nabla^s\boldsymbol{w} : 2\nu\nabla^s\boldsymbol{u}\,\mathrm{d}\Omega \tag{12}$$

$$c\left(\boldsymbol{u};\boldsymbol{w},\boldsymbol{u}\right)_{\Omega} = \int_{\Omega} \boldsymbol{w}\cdot\left(\boldsymbol{u}\cdot\nabla\boldsymbol{u}\right)\,\mathrm{d}\Omega \tag{13}$$

2.4 Time integration

The time integration scheme adopted to solve the Navier-Stokes equations is the Newmark method, where the velocity derivative with respect to time at time level $n+1$ can be written as

$$\dot{\boldsymbol{u}}^{n+1} = \frac{1}{\gamma}\frac{\left(\boldsymbol{u}^{n+1}-\boldsymbol{u}^{n}\right)}{\Delta t} - \frac{(1-\gamma)}{\gamma}\dot{\boldsymbol{u}}^{n}, \tag{14}$$

where $\gamma = 1/2$ is adopted as the Newmark parameter in order to obtain second-order convergence in time. Rewriting the weak form of the Navier-Stokes equation in Eq. (11),

$$\begin{aligned}\Big\{ \left(\boldsymbol{w},\boldsymbol{u}\right)_{\Omega} + \gamma\Delta t\big[c\left(\boldsymbol{u};\boldsymbol{w},\boldsymbol{u}\right)_{\Omega} + a\left(\boldsymbol{w},\boldsymbol{u}\right)_{\Omega} - \left(\nabla\cdot\boldsymbol{w},p\right)_{\Omega} + \left(q,\nabla\cdot\boldsymbol{u}\right)_{\Omega} - \left(\boldsymbol{w},\bar{\boldsymbol{t}}\right)_{\Gamma_t} - \\ - \left(\boldsymbol{w},\boldsymbol{b}\right)_{\Omega}\big]\Big\}^{n+1} = \left(\boldsymbol{w},\boldsymbol{u}^{n}\right)_{\Omega} + (1-\gamma)\,\Delta t\left(\boldsymbol{w},\dot{\boldsymbol{u}}^{n}\right)_{\Omega},\ \forall\left(\boldsymbol{w},q\right).\end{aligned} \tag{15}$$

2.5 Finite Element discretization

This work adopts a mixed formulation so that the fluid finite elements have two unknowns (velocity and pressure) as primitive variables and the Lagrange multipliers are additional unknowns that must be discretized along the interface. The approximation functions for the velocities and pressure, defined locally inside a finite element domain Ω_e, can be defined as

$$\boldsymbol{u}^h\left(\boldsymbol{x}\right)\big|_{\boldsymbol{x}\in\Omega_e} = \mathbf{N}_u\mathbf{u}_e \quad \text{and} \quad p^h\left(\boldsymbol{x}\right)\big|_{\boldsymbol{x}\in\Omega_e} = \mathbf{N}_p\mathbf{p}_e \tag{16}$$

respectively. $\mathbf{N}_u$ and $\mathbf{N}_p$ are the shape functions for the velocity and pressure, respectively and $\mathbf{u}_e$ and $\mathbf{p}_e$ its nodal values. The test functions are defined in a similar way by

$$\boldsymbol{w}^h\left(\boldsymbol{x}\right)\big|_{\boldsymbol{x}\in\Omega_e} = \mathbf{N}_u\mathbf{w}_e \quad \text{and} \quad q^h\left(\boldsymbol{x}\right)\big|_{\boldsymbol{x}\in\Omega_e} = \mathbf{N}_p\mathbf{q}_e \tag{17}$$

In this work, in order to not violate the LLB compatibility condition for mixed problems, it was used a Taylor-Hood P2-P1 element (quadratic interpolation in velocity and linear interpolation in pressure) as illustrated in Fig. 1.

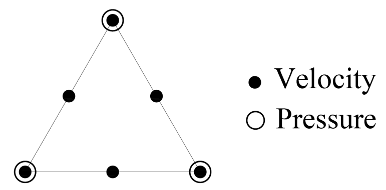

Figure 1: P2-P1 Taylor Hood element.

After some algebraic manipulations of the equations demonstrated in previous sections and using the Finite Element discretization just presented we have

$$\begin{cases}\dfrac{\mathbf{M}}{\gamma\Delta t}\mathbf{u}^{n+1} + \left[\mathbf{C}\left(\mathbf{u}^{n+1}\right)+\mathbf{K}\right]\mathbf{u}^{n+1} + \mathbf{G}\mathbf{p}^{n+1} & = \mathbf{f}^{n+1} + \dfrac{\mathbf{M}}{\gamma\Delta t}\mathbf{u}^{n} + \dfrac{1-\gamma}{\gamma}\mathbf{M}\dot{\mathbf{u}}^{n} \\ \mathbf{G}^{\mathsf{T}}\mathbf{u}^{n+1} & = 0\end{cases} \tag{18}$$

where the local matrices are defined as

$$\mathbf{M}_e = \int_{\Omega_e} \mathbf{N}_u^{\mathsf{T}} \mathbf{N}_u \mathrm{d}\Omega_e \qquad \text{Mass matrix}$$

$$\mathbf{K}_e = \int_{\Omega_e} \mathbf{B}_u^{\mathsf{T}} \nu \mathbf{B}_u \mathrm{d}\Omega_e \qquad \text{Viscous matrix}$$

$$\mathbf{C}_e = \int_{\Omega_e} \mathbf{N}_u^{\mathsf{T}} \left[(\mathbf{N}_{u,i} \mathbf{u}_e) \otimes \mathbf{e}_i \right] \mathbf{N}_u \mathrm{d}\Omega_e \qquad \text{Convective matrix}$$

$$\mathbf{G}_e = -\int_{\Omega_e} (\nabla \cdot \mathbf{N}_u)^{\mathsf{T}} \mathbf{N}_p \mathrm{d}\Omega_e \qquad \text{Gradient operator}$$

$$\mathbf{G}_e^{\mathsf{T}} \qquad \text{Divergent operator}$$

$$\mathbf{f}_e = \int_{\Gamma_{te}} \mathbf{N}_u^{\mathsf{T}} \bar{\mathbf{t}} \mathrm{d}\Gamma_{te} + \int_{\Omega_e} \mathbf{N}_u^{\mathsf{T}} \mathbf{b} \mathrm{d}\Omega_e \qquad \text{Field forces and boundary conditions}$$

2.6 Interface

The strategy adopted in this work is to use embedded interfaces in FSI simulations to compute the fluid flow variables from a Eulerian fixed mesh. The fluid mesh is defined over the fluid domain and extends totally into the structural domain or into some portion of it, as shown in Fig. 2.

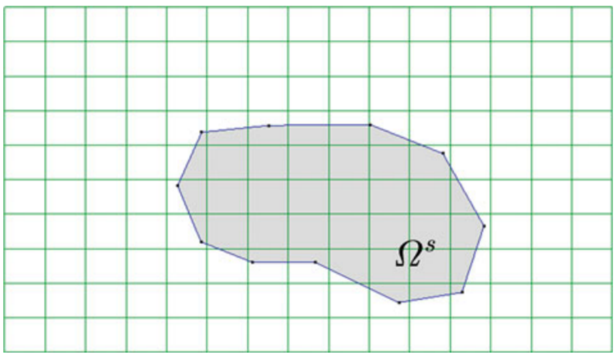

Figure 2: Typical fluid mesh for embedded interface approach.

For that reason, the structure's wet surface, in general, does not match the fluid grid nodes, hence the fluid velocities at the interface must be weakly enforced. We define a domain that contains the fluid Ω^f and the structural Ω^s (Fig. 3). Γ^i is the interface between the fluid and the structure domains and $\boldsymbol{n}^f$ and $\boldsymbol{n}^s$ their respective unit outward normal vectors.

Now, to ensure the fluid velocity compatibility at the interface, we must have, for a non-slip interface type,

$$\boldsymbol{u}^f = \dot{\boldsymbol{d}}^s = \overline{\boldsymbol{u}}^i \qquad \forall \boldsymbol{x} \in \Gamma^i, \tag{19}$$

$$\boldsymbol{T}^f \boldsymbol{n}^f = -\boldsymbol{T}^s \boldsymbol{n}^s \qquad \forall \boldsymbol{x} \in \Gamma^i \tag{20}$$

where Eq. 19 is the kinematic interface condition, $\dot{\boldsymbol{d}}$ is the structure velocity and Eq. 20 represents the dynamic condition. The superscripts on these equations distinguish the variables form the different domains (fluid and structure).

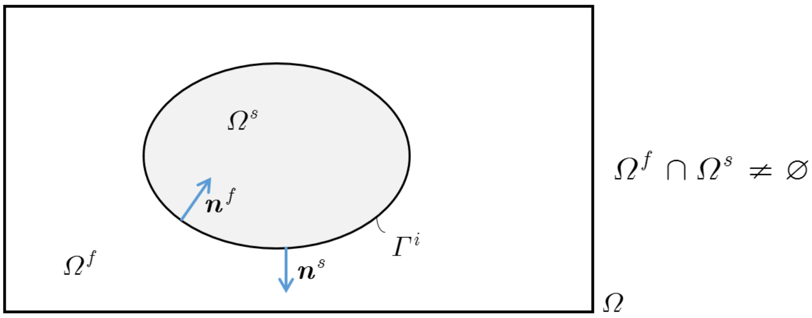

Figure 3: Fluid and structural domains.

The imposition of Eq. 19 in the fluid problem can be done using Lagrange multipliers. Therefore, it is possible to define a functional given by

$$\Pi = \left(\boldsymbol{\lambda}, \boldsymbol{u}^f - \dot{\boldsymbol{d}}^s\right)_{\Gamma^i} \tag{21}$$

where λ represents the Lagrange multiplier of condition Eq. 19 and constitutes an additional variable field for the problem. The Lagrange multiplier can be identified as a traction acting along Γ^i. The variational form of this function, considering the structure movement to be known *a priori* at the time of solving the fluid problem, is

$$\delta\Pi = \left(\delta\boldsymbol{\lambda}, \boldsymbol{u}^f - \dot{\boldsymbol{d}}^s\right)_{\Gamma^i} + \left(\boldsymbol{\lambda}, \delta\boldsymbol{u}^f\right)_{\Gamma^i}. \tag{22}$$

These terms must be added to the weak form presented in Eq. 15. Thus we have

$$\begin{aligned} \Big\{ (\boldsymbol{w}, \boldsymbol{u})_{\Omega^f} + \gamma\Delta t\big[c\,(\boldsymbol{u}; \boldsymbol{w}, \boldsymbol{u})_{\Omega^f} + a\,(\boldsymbol{w}, \boldsymbol{u})_{\Omega^f} - (\nabla\cdot\boldsymbol{w}, p)_{\Omega^f} + (q, \nabla\cdot\boldsymbol{u})_{\Omega^f} - \\ - \left(\boldsymbol{w}, \bar{\boldsymbol{t}}\right)_{\Gamma_t} - \left(\delta\boldsymbol{\lambda}, \boldsymbol{u} - \overline{\boldsymbol{u}}^i\right)_{\Gamma^i} - (\boldsymbol{w}, \boldsymbol{\lambda})_{\Gamma^i} - (\boldsymbol{w}, \boldsymbol{b})_{\Omega^f}\big]\Big\}^{n+1} = \\ = (\boldsymbol{w}, \boldsymbol{u}^n)_{\Omega^f} + (1-\gamma)\,\Delta t\,(\boldsymbol{w}, \dot{\boldsymbol{u}}^n)_{\Omega^f}\,,\ \forall\,(\delta\boldsymbol{\lambda}, \boldsymbol{w}, q) \end{aligned} \tag{23}$$

where the convective and viscous terms defined in Eq. 11 are restricted to Γ^i.

2.7 Discretization of the interface

The discretization of the interface can be done in several ways. The most intuitive and adopted technique is to define nodes at the intersections between the interface and the fluid elements. These nodes are then used to define the Lagrange multipliers' nodal values, and some appropriate approximating functions are used to interpolate the values along the interface. In our simulations, the adoption of low-order finite elements has shown a high sensibility to numerical instabilities in the Lagrange multiplier results.

In order to address this problem, we propose an alternative technique to discretize the interface independently of the fluid mesh (Gomes, 2015). Additionally, discontinuous piecewise constant shape functions were adopted to simplify the implementation. The schematic discretization of the interface is shown in Fig. 4, where the structured mesh consists of quadrilateral fluid elements.

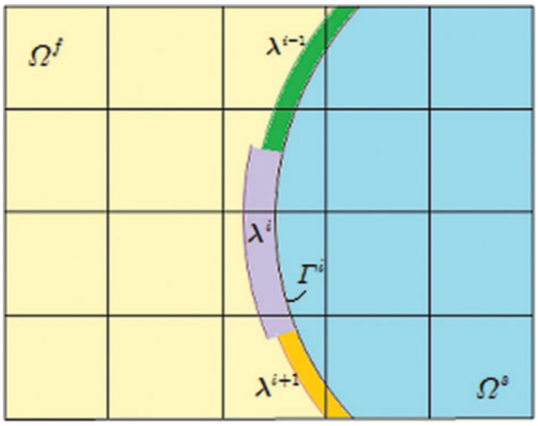

Figure 4: Discretization of the interface between the riser and the fluid.

The approximating and test functions of the Lagrange multipliers can be defined as

$$\boldsymbol{\lambda}^h(\boldsymbol{x})\big|_{\boldsymbol{x}\in\Gamma_e^i} = \mathbf{N}_\lambda \boldsymbol{\lambda}_e \quad \text{and} \quad \delta\boldsymbol{\lambda}^h(\boldsymbol{x})\big|_{\boldsymbol{x}\in\Gamma_e^i} = \mathbf{N}_\lambda \delta\boldsymbol{\lambda}_e \tag{24}$$

$\mathbf{N}_\lambda$ is the shape function of the Lagrange multipliers.

2.8 Integration cells

In order to compute the integrals over cut elements, we subdivide the element that belongs both to the fluid and structural domain into triangular integrating cells, as shown in Fig. 5, for a triangular and quadrilateral fluid element. Inside the fluid element, the interface is approximated by a straight line. This approximation is very common in the Finite Element Method and leads to an error that converges to zero as the elements' size decreases.

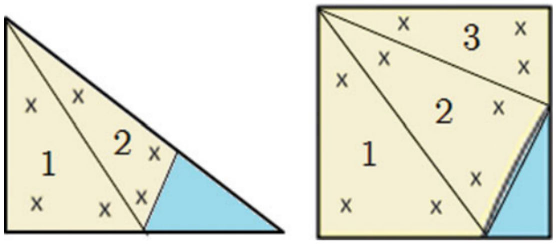

Figure 5: Integration over cut elements. The Gauss points are represented by "x" symbol.

3 RISER

Many elements in an offshore oil exploitation plant can be modeled as long beams. Some examples are ropes, umbilical cables, flexible and rigid pipes and hoses. Many of these are composite structures. There are mainly two different modeling scales for these structures: local and global analysis. The first one usually is related to local stress predictions, interactions between the structural components and, usually, is focused on a given cross section that is very detailed in the model. The second scale considers the whole structure behavior. A structural theory is usually adopted based on the expected local behavior, such as a beam theory. Then, the global loads are applied and the internal loads are obtained for each location of the global model. Both scales analysis are complementary.

This work is focused on the global models of risers. These can be rigid or flexible pipes or umbilical cables, submerged and with one extreme point fixed in a floating unit and the other in the seabed. They are subjected to environment loads, such as their self-weight, buoyancy, sea current drag and sea wave excitation.

Some riser configurations have a region laid in the seabed, named “flowline”. In this work, for nomenclature simplification, the set given by riser plus flowline will be named simply as “riser”.

3.1 Geometrically-exact 3d static beam model

A Timoshenko or first-order shear beam model was assumed to represent the 3D structure of the riser. Thus, it is possible to consider tension, compression and shear loads, and bending and torsion moments. Actually the riser problem usually has no important shear effects in the beam, due to the structure slenderness. Due to the nature of the geometrically-exact formulation here used, however, this effect was naturally included in the model, once no constraints to the movement in space of each cross section were made.

Large displacements and large rotations of the beam cross sections are considered, so the model is geometrically nonlinear.

For a complete explanation of the structural model, refer to Gay Neto et al. (2014).

3.2 Contact model

The contact model captures the transition between sliding/rolling effects, including the moment of friction forces in the equations and using the beam rotational degrees of freedom (DOFs) to describe contact kinematics.

Defining some variables:

- $\boldsymbol{c}$ is the contact force acting at a point $\boldsymbol{P}$;
- $\boldsymbol{n}$ is the normal direction of contact interface;
- $\boldsymbol{f}$ is the tangential component of contact force (friction);
- P_f is the power of the friction force;
- $\boldsymbol{v}_P$ is the velocity of a point $\boldsymbol{P}$;
- $\boldsymbol{v}_C$ is the velocity of a point $\boldsymbol{C}$;
- $\boldsymbol{\omega}$ is the angular velocity vector of a cross section of the riser (considered as a rigid body);
- $\boldsymbol{M}_f$ is the moment of friction force related to pole $\boldsymbol{C}$.

It is possible to write the power of friction force expression by:

$$P_f = \boldsymbol{f} \cdot \boldsymbol{v}_P = \boldsymbol{f} \cdot [\boldsymbol{v}_C + \boldsymbol{\omega} \times (\mathbf{P} - \boldsymbol{C})] = \boldsymbol{f} \cdot \boldsymbol{v}_C + \boldsymbol{f} \cdot \boldsymbol{\omega}\,(\boldsymbol{P} - \boldsymbol{C}) = \boldsymbol{f} \cdot \boldsymbol{v}_C + \boldsymbol{M}_f \cdot \boldsymbol{\omega}. \quad (25)$$

With that, when transporting friction force to the centroid of the cross section (necessary to use a structural beam model), there are two contributions from friction to the system: on forces and on moments. Both are related to friction loading applied to each cross section of the riser.

Most of the models implemented in analysis software disregard the second term, once consider usually "node to surface" or "surface to surface" approach, through a classical tangential gap in contact definition.

More details about the contact model can be found in Gay Neto et al. (2014) and Gay Neto et al. (2015).

3.3 Structural model

The base of the static structural model for the riser is completely described in Gay Neto et al. (2014). Some basic assumptions are presented here for self-containing of the present work. Beam elements in a finite element approximation are used to represent the riser structure. Large displacements and rotations are considered in this geometrically nonlinear model. Cross sections are considered to be rigid, but not remaining orthogonal to beam axis, that is, the kinematics of a Timoshenko beam formulation is assumed. The movement of each cross section is considered with no theoretical magnitude limitation to displacement and finite rotations. Rodrigues' rotation parameters are adopted, constructing a rotation tensor for each cross section to describe its orientation when the beam structure is deformed. Furthermore, to avoid large values of rotations, which could cause singularities in the rotation tensor, an updated Lagrangian framework is used to describe kinematics. Then, theoretically unlimited magnitude of rotations can be solved with no singularity problems. This model can be described as a geometrically-exact formulation of beams.

The riser material model is assumed to be linear and elastic, which is the simplest constitutive model. The main interest of this work is to investigate contact and geometric nonlinearities effects in structural riser analysis. Eventually, more realistic material models could be added. The external loads considered in this work are the self-weight of the riser and the fluid forces in the structure, described in previous sections.

4 METHODOLOGY OF ANALYSIS

This section describes the methodology used to investigate hydrodynamics over the riser, and also the riser-seabed interaction. Simulations were performed using two in-house finite element codes, based on theory presented in previous sections.

For the FSI solver, the code is named HPC LMC (High Performance Computing at University of São Paulo Computational Mechanics Laboratory) and for the riser solver the code is named GIRAFFE (Generic Interface Readily Accessible for Finite Elements). Figure 6 illustrates this interaction between the two solvers.

Both solvers are implemented using C++ language and make use of parallel modules in order to achieve the best overall performance.

The steps that must be executed in order to have the complete FSI problem solved are:

1. Execute GIRAFFE and choose the correct Neutral File;
    - Neutral File consists in a file that has its content (e.g. nodes coordinates, element connectivity, material properties, time step, simulation time) and format standardized in such a way that a particular solver is capable of executing different problems (e.g. steady, unsteady state problem) with the same source code.

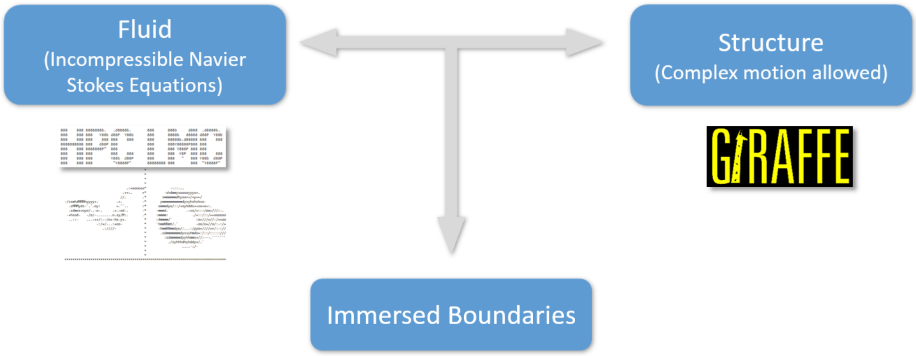

Figure 6: Interaction between the two solvers.

2. GIRAFFE will solve the static problem and provide the base riser catenary as illustrated in Fig. 7;
3. Execute HPC LMC solver with the fluid Neutral File that will solve the transient problem until the velocity of the fluid is stable;
4. Do for each time step:
   (a) Since the FSI code is implemented for 2D problems it is necessary to simulate the 3D problem as several horizontal 2D planes. Each plane will be responsible for finding the forces generated for that particular depth and send to GIRAFFE. Execute HPC LMC solver that will solve the transient problem for each plane until all of them get converged;
   (b) Execute GIRAFFE to solve the riser structure for the nodal loads applied from the fluid over the riser structure until it is converged;
   (c) Increase the solution time with the time step defined in the numerical simulation and reexecute item 4.
5. The final configuration after a specific amount of time is illustrated in Fig. 7.

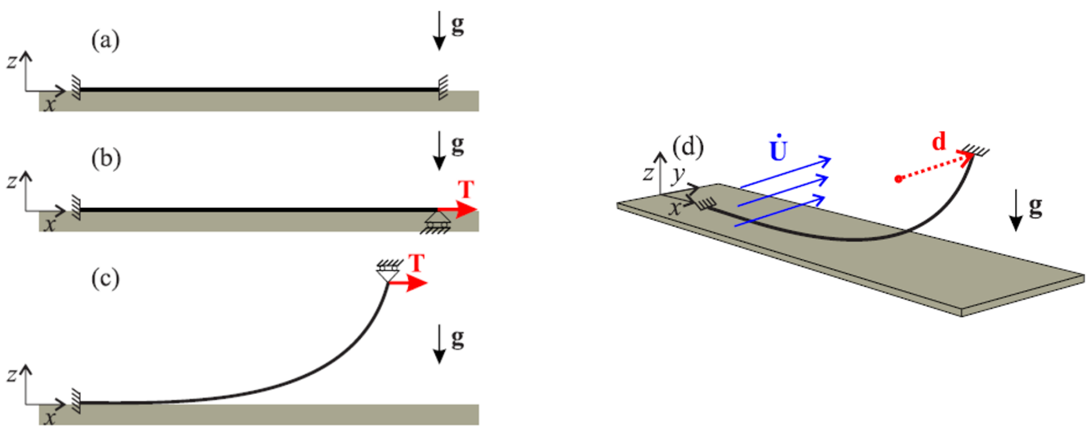

Figure 7: Steps used to solve the numerical model sequentially (a), (b) and (c) to obtain the base catenary and (d) final configuration after sea current imposition (Gay Neto et al., 2015).

5 NUMERICAL SIMULATIONS

This section presents some simulations in order to test the integration between the two solvers and the formulation presented (FSI and geometrically-exact beam theory). The FSI was applied to a riser structure with seabed contact with the following properties:

Table 1: Riser and seawater physical properties (Gay Neto et al., 2015).

Riser length	$5000.00\,\mathrm{m}$
Axial stiffness	$6.08\,\mathrm{GN}$
Bending stiffness	$110.80\,\mathrm{MN\,m^2}$
Torsion stiffness	$85.20\,\mathrm{MN\,m^2}$
Shear stiffness	$2.34\,\mathrm{GN}$
Water depth	$1709.00\,\mathrm{m}$
Water density	$1000.00\,\mathrm{kg/m^3}$
Sea current speed	$0.50\,\mathrm{m/s}$

The properties of the fluid and the parameters used for the simulation are:

Table 2: Fluid properties and parameters used for the simulation.

Density	$1.00\,\mathrm{kg/m^3}$
Dynamic Viscosity	$2.00\times10^{-4}\,\mathrm{Pa\cdot s}$
Inlet Velocity	$0.50\,\mathrm{m/s}$
Reynolds	100 (Laminar Flow)
Time step	$0.05\,\mathrm{s}$
Maximum Physical Time	$10.00\,\mathrm{s}$

It is worth pointing out that the FSI solver was developed, initially, for problems with low Reynolds number and to verify the theory of Immersed Boundaries with Lagrange multipliers (Gomes, 2015). Taking this into consideration, the physical properties (density and dynamic viscosity) were modified to have a laminar flow around the riser and therefore no stabilization issue should raise. Additionally, the idea of this work was to evaluate and demonstrate the applicability of using a staggered scheme with two different solvers (HPC LMC and GIRAFFE). In order to study different and more complex problems (e.g. VIV) further implementations and development are required.

5.1 Geometry

Figure 8 shows the gometry of the model used in the numerical examples and simulations.

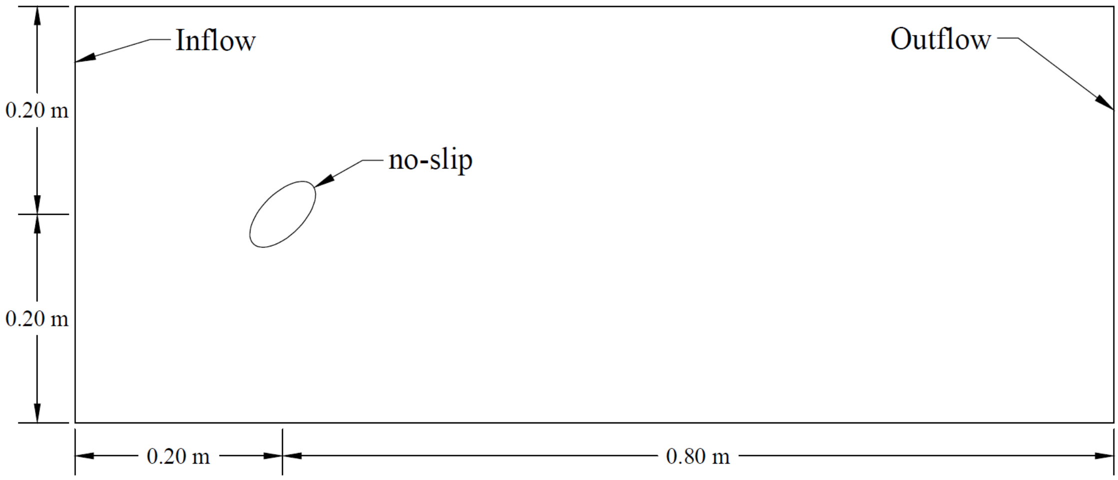

Figure 8: Horizontal plane geometry.

Table 3 shows the finite element discretization for this geometry.

Table 3: Model properties.

Base Size of Mesh	$0.015\,\mathrm{m}$
Number of elements	57 230
Number of nodes	115 161

5.2 2D FSI simulation

In order to simulate the sea current applied to the riser, it was created several horizontal planes at different depths. Each plane is positioned according to riser position at that depth and is responsible for solving the FSI and send the resultant forces and moments to GIRAFFE.

Since the planes are horizontal, the section cut between the plane and the riser results in an ellipse (Fig. 9).

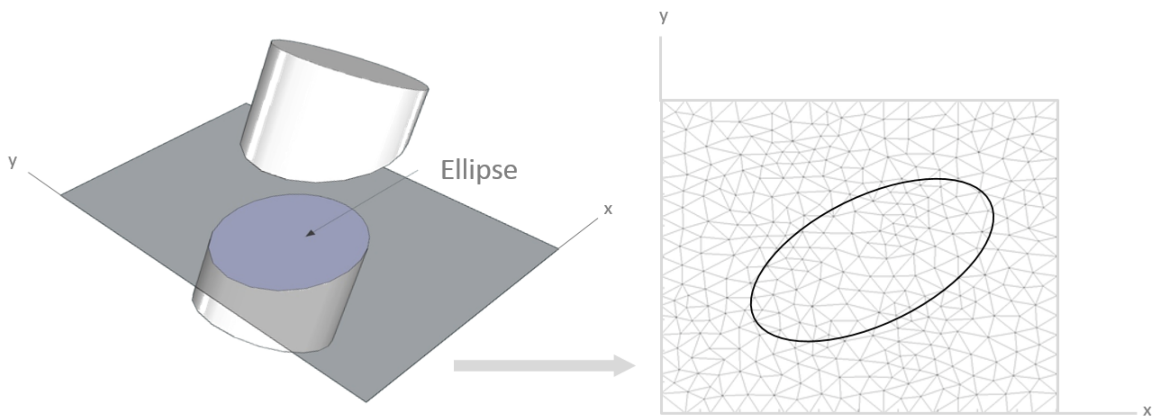

Figure 9: Riser section cut.

The GIRAFFE implementation code has a C++ method that returns the current (at a given instant) tangent vector for a specific node (Fig. 10a).

With this vector it is possible to find all parameters of the rotated ellipse as demonstrated in Fig. 10b.

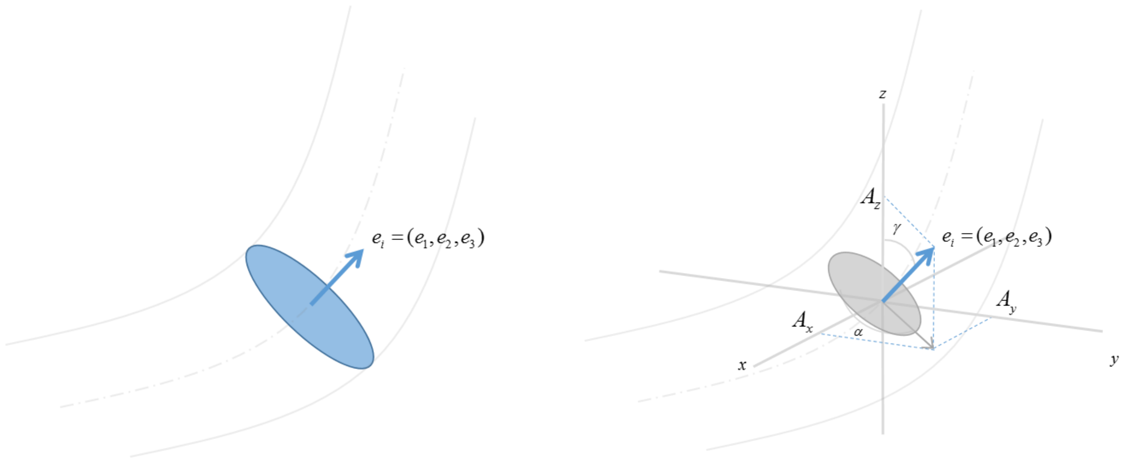

(a) Tangential vector. **(b) Ellipse parameters.**

Figure 10: Tangent vector and ellipse parameters.

5.3 Analytical solution

There are two different approaches that we could use to generate the structural domain. Use a structural mesh or use an analytical equation for the ellipse.

Since it is not possible to know *a priori* the position of the riser at a specific depth, the best approach, and the one used in this work, was to make use of the anlytical equation. The next section will demonstrate the equations and interface definition of the riser over the fluid domain.

5.4 Rotated ellipse equation

Assume we have an ellipse with horizontal radius h and vertical radius v, centered at the origin (Fig. 11a).

The equation for the non-rotated ellipse is:

$$\frac{x^2}{h^2} + \frac{y^2}{v^2} = 1 \tag{26}$$

where x and y are the coordinates of points on the ellipse.

Using the equations for rotating a point over the origin by an angle α (counter-clockwise), we get:

$$x_r = x \cos\alpha + y \sin\alpha \tag{27}$$

$$y_r = y \cos\alpha - x \sin\alpha \tag{28}$$

Plugging these equations into Eq. 26 for the non-rotated ellipse, we get the equation for a rotated ellipse (Fig. 11b):

$$\frac{(x\cos\alpha + y\sin\alpha)^2}{h^2} + \frac{(y\cos\alpha - x\sin\alpha)^2}{v^2} = 1 \tag{29}$$

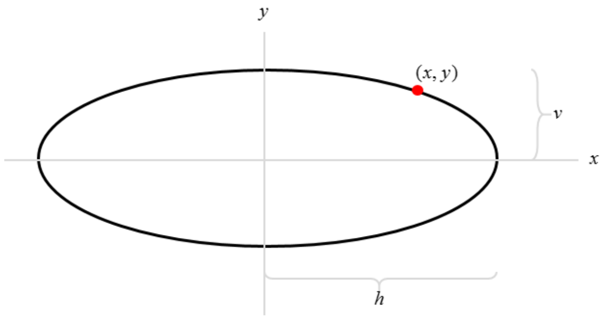

(a) Ellipse.

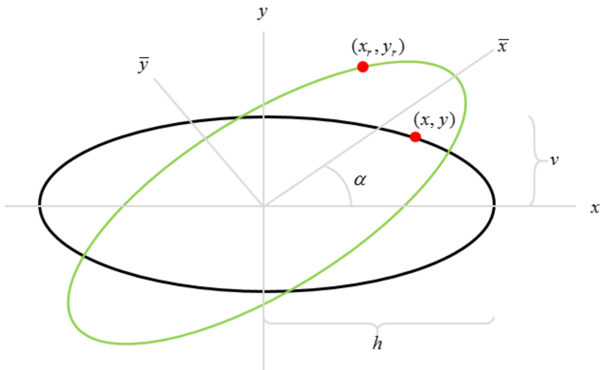

(b) Rotated ellipse.

Figure 11: Ellipse and rotated ellipse.

5.5 Intersection line

It is necessary to find the intersection nodes between the rotated ellipse and the fluid meshes. These intersection nodes will define the interface moving boundary.

To find the intersection nodes we use the following equation:

$$x_{int} = \frac{-b \pm \sqrt{b^2 - 4ac}}{2a} \tag{30}$$

where

$$a = v^2\left(\cos^2\alpha + 2m\cos\alpha\sin\alpha + m^2\sin^2\alpha\right) + h^2\big(m^2\cos^2\alpha - \\ -2m\cos\alpha\sin\alpha + \sin^2\alpha\big) \tag{31}$$

$$b = 2v^2 b_1\left(\cos\alpha\sin\alpha + m\sin^2\alpha\right) + 2h^2 b_1\left(m\cos^2\alpha - \cos\alpha\sin\alpha\right) \tag{32}$$

$$c = b_1^2\left(v^2\sin^2\alpha + h^2\cos^2\alpha\right) - h^2v^2 \tag{33}$$

Plugging into the equation of the line:

$$y = mx + b_1 \tag{34}$$

it is possible to find the nodes of intersection between the ellipse and the fluid meshes.

Figures 12a and 12b illustrate the intersection line and the moving boundary after finding the intersection nodes and disabling the fluid meshes inside the structural domain.

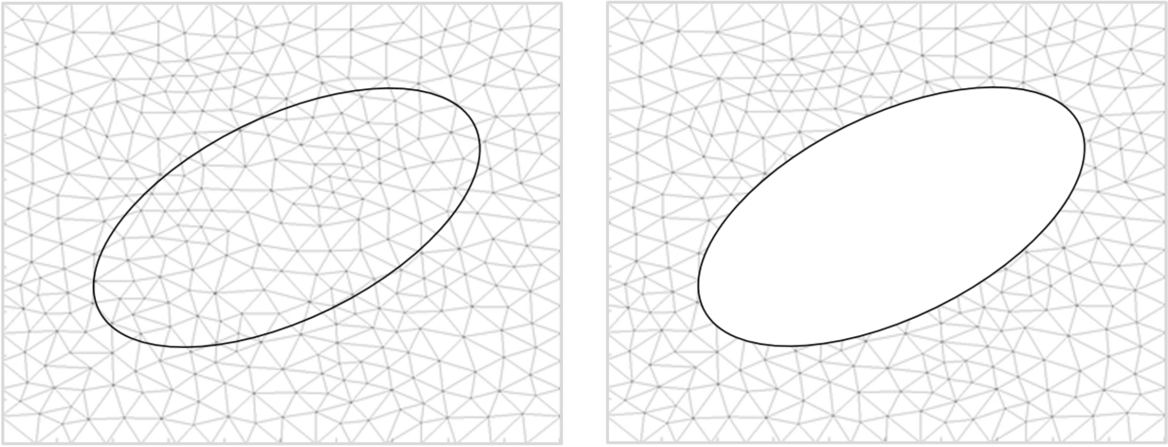

(a) Intersection line. **(b) Moving boundary.**

5.6 Lagrange multipliers forces

The forces that are applied to the riser are given by the Lagrange multipliers and Fig. 13 illustrate how the forces and moment vectors are calculated.

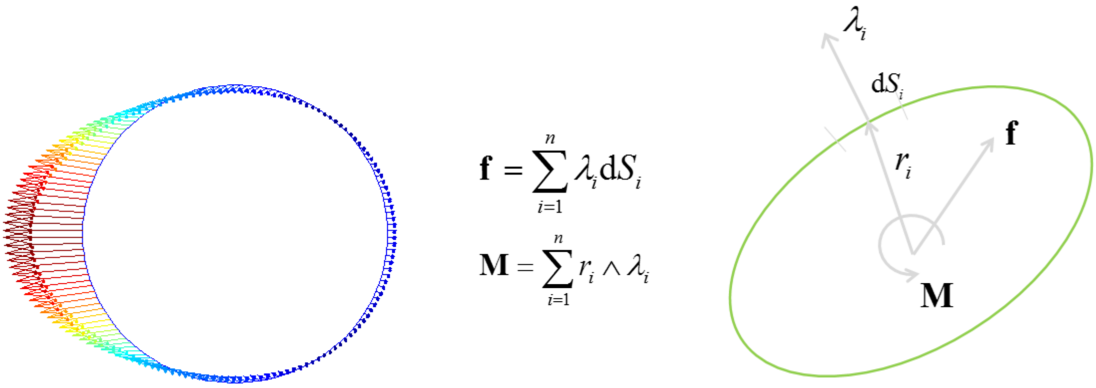

$$\mathbf{f} = \sum_{i=1}^{n} \lambda_i \mathrm{d}S_i$$

$$\mathbf{M} = \sum_{i=1}^{n} r_i \wedge \lambda_i$$

Figure 13: Lagrange multipliers forces vector that are sent to GIRAFFE solver.

5.7 Steady state problem

In order to test the analytical solution of the ellipse with the FSI solver, it was simulated the flow past a ridig ellipse (simulating the section cut between the horizontal plane and the riser) with a steady state flow.

The parameters used for this example are:

Table 4: Parameters used for the steady state problem.

Inlet Velocity	$0.20\,\mathrm{m/s}$
Reynolds	40 (Laminar Flow)

Results

Figure 14 shows the results (velocity and pressure) of the numerical example.

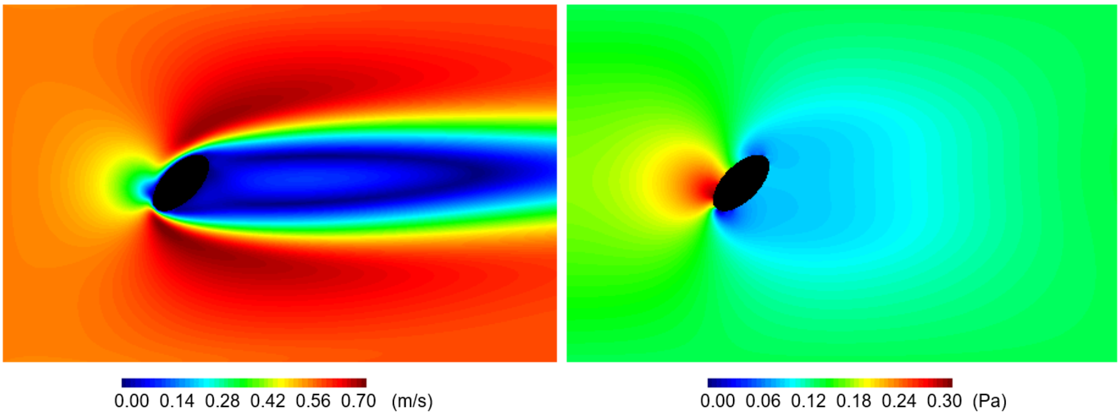

Figure 14: Flow past a rigid ellipse; Crossflow velocity (left) and pressure (right) at $Re = 40$.

5.8 Unsteady state problem

For the unsteady state problem it was used the same geometry, fluid properties, parameters of the simulation and the methodology of analysis as described in previous sections. It was used a time-varying inflow velocity ranging from 0.00 to $0.50\,\mathrm{m/s}$ at the first two seconds and then a $0.50\,\mathrm{m/s}$ constant inflow velocity until the end of the simuation ($T = 10.00\,\mathrm{s}$).

Results

First it is illustrated the velocity at $t = 2.00\,\mathrm{s}$ with a constant inflow velocity of $0.50\,\mathrm{m/s}$. Then, for each horizontal FSI plane, it is illustrated the velocity and pressure at different instant of times ($t = 6.00\,\mathrm{s}$, $t = 7.50\,\mathrm{s}$ and $t = 9.00\,\mathrm{s}$) and depths ($Z = 100.00\,\mathrm{m}$ and $Z = 400.00\,\mathrm{m}$).

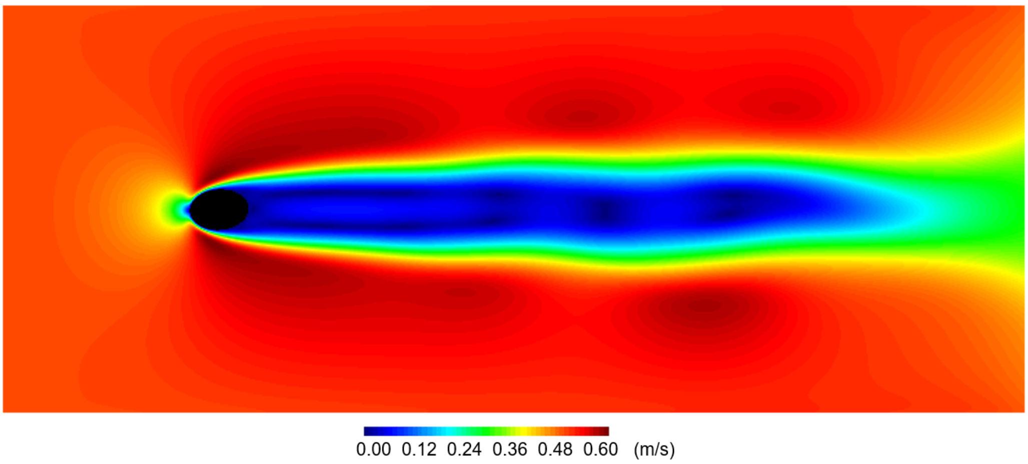

Figure 15: Crossflow velocity at $t = 2.00\,\mathrm{s}$ and $Z = 100.00\,\mathrm{m}$.

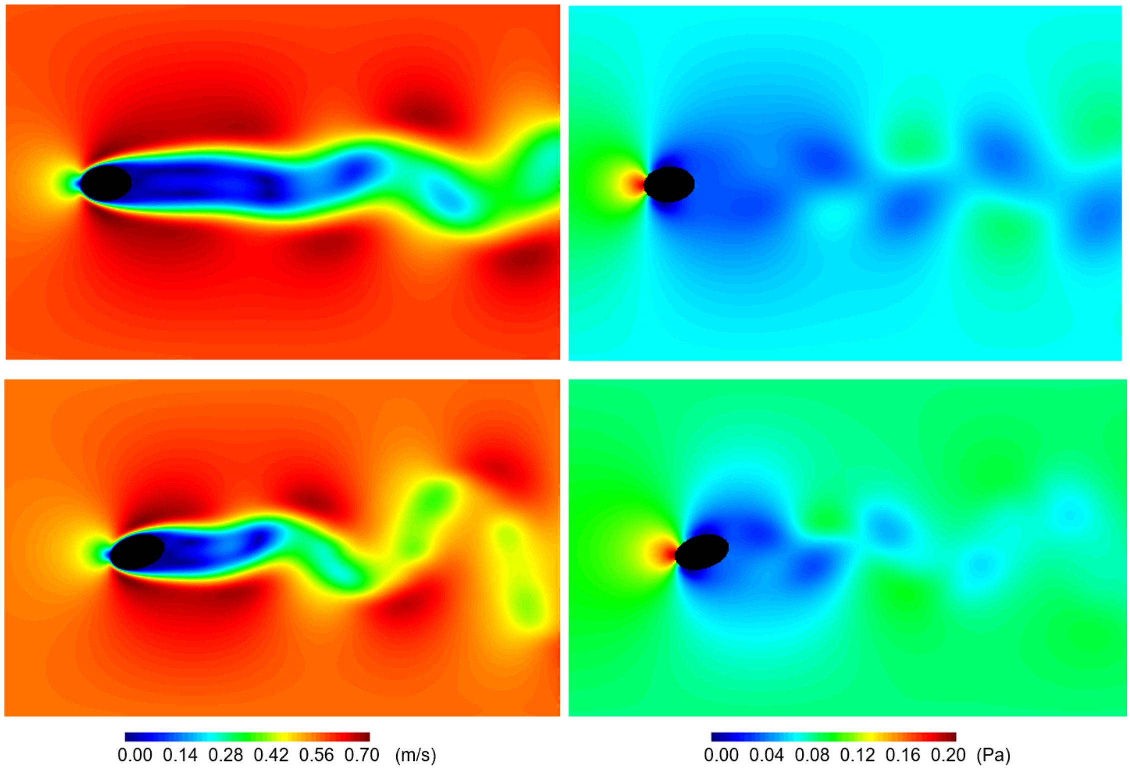

Figure 16: Flow past riser section cut; Crossflow velocity (left) and pressure (right) at $Re = 100$, $t = 6.00\,\mathrm{s}$; Depths $Z = 100.00\,\mathrm{m}$ (top) and $Z = 400.00\,\mathrm{m}$ (bottom).

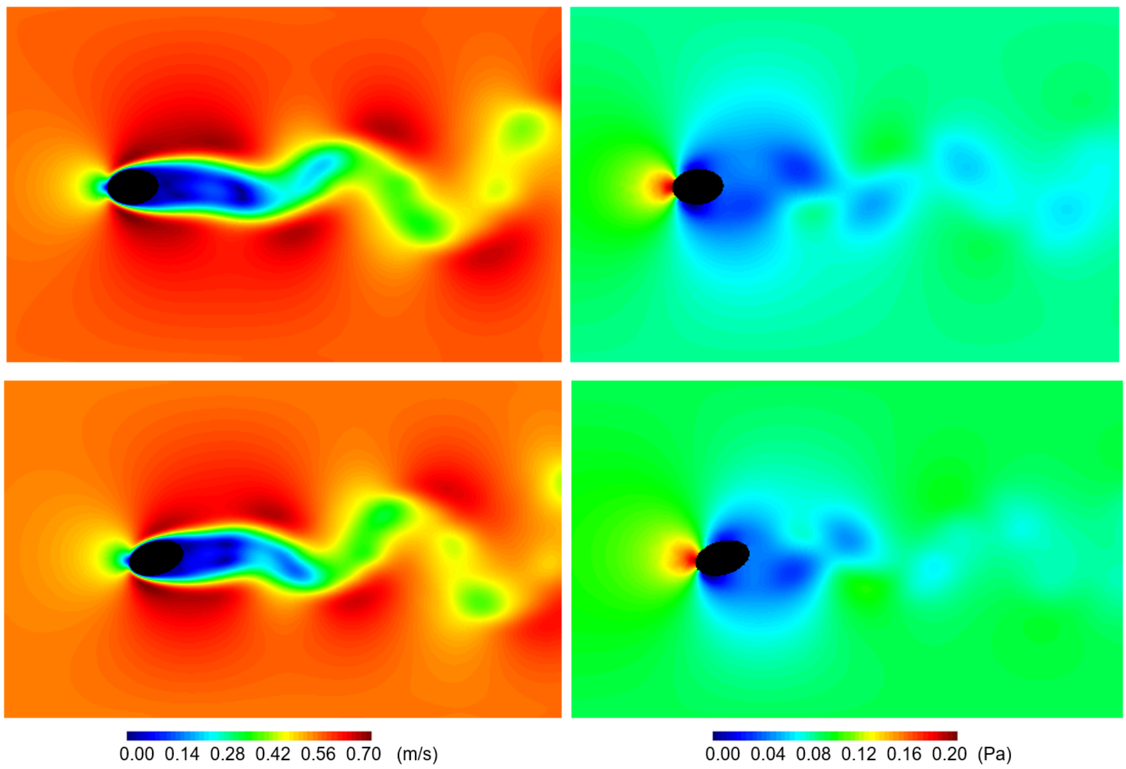

Figure 17: Flow past riser section cut; Crossflow velocity (left) and pressure (right) at $Re = 100$, $t = 7.50\,\mathrm{s}$; Depths $Z = 100.00\,\mathrm{m}$ (top) and $Z = 400.00\,\mathrm{m}$ (bottom).

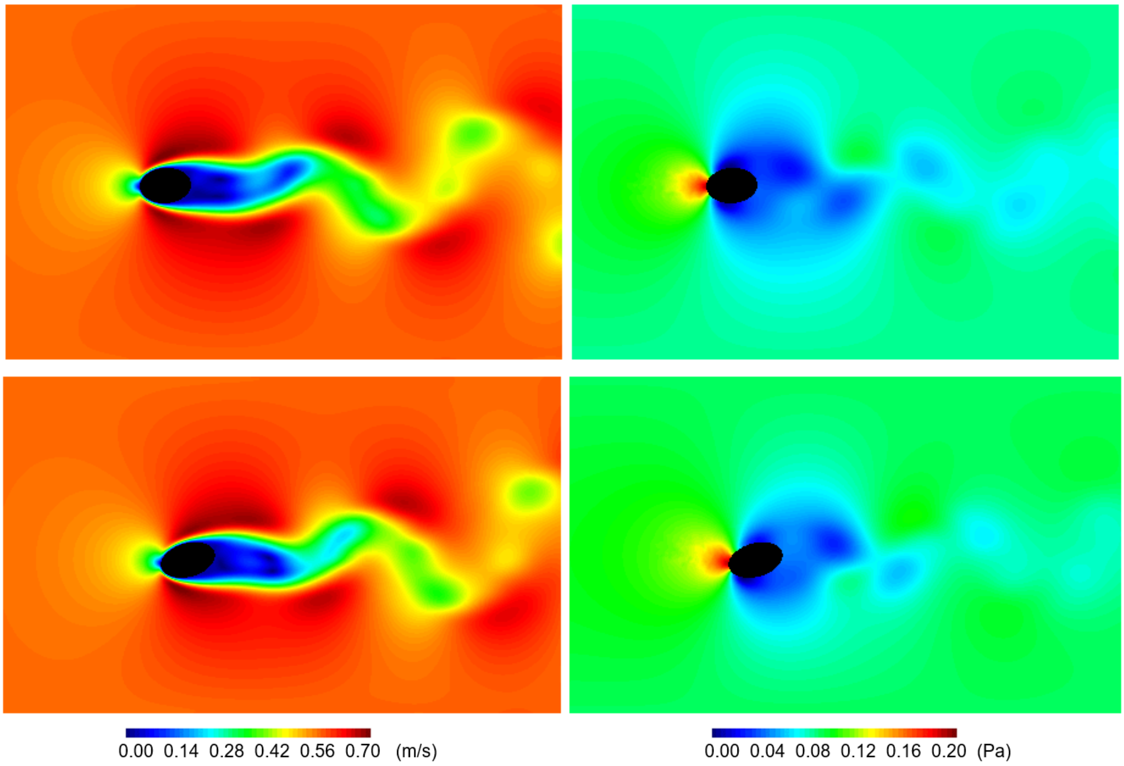

Figure 18: Flow past riser section cut; Crossflow velocity (left) and pressure (right) at $Re = 100$, $t = 9.00\,\mathrm{s}$; Depths $Z = 100.00\,\mathrm{m}$ (top) and $Z = 400.00\,\mathrm{m}$ (bottom).

6 CONCLUSION

This work has presented the integration between two different solvers, a FSI and a geometrically-exact beam solver in order to study the hydrodynamics over a riser with seabed contact. Although it is necessary to implement a stabilization scheme for convection dominated flows and also a turbulence model to represent the model in a more realistic way, the integration between the two solvers was successfully accomplished. This work is in its initial stage of development and in the future it could help researchers to study the VIV over a riser easily using the newest theories, either in Immersed Boundary methods, or in geometrically-exact beam theories.

7 FUTURE WORK

In order to have the VIV study possible we need to implement the following routines in the FSI solver:

- Implement a stabilization scheme (e.g. SUPG and PSGP);
- Implement a turbulence model;

Another possibility is to implement a 3D model for fluids, once the actual flow is 3D and we are here approximating this behavior by a set of 2D flows, which is not fully realistic.

REFERENCES

Baiges, J., Codina, R., Henke, F., Shahmiri, S., Wall, W. A., 2012. A symmetric method for weakly imposing Dirichlet boundary conditions in embedded finite element meshes. *International Journal for Numerical Methods in Engineering*, vol. 90, p. 636-658.

Elias, R. N., Gonçalves, Jr. M. A., Coutinho, A. L. G. A., Esperança, P. T. T., Martins, M. A. D., Ferreira, M. D. A. S., 2009. Computational Techniques for Stabilized Edge-Based Finite Element Simulation of Nonlinear Free-Surface Flows. *Journal of Offshore Mechanics and Arctic Engineering*, vol. 131, p. 041103-0411-7.

Forster, C., Wall, W. A., Ramm, E., 2007. Artificial added mass instabilities in sequential staggered coupling of nonlinear structures and incompressible viscous flows. *Computer Methods in Applied Mechanics and Engineering*, vol. 196, p. 1278-1293.

Gay Neto, A., Pimenta, P. M., 2013. Static analysis of offshore risers with a geometrically-exact 3D beam model subjected to unilateral contact. *Computational Mechanics*, vol. 53, p. 125-145.

Gay Neto, A., Pimenta, P. M., Wriggers, P., 2014. Contact between rolling beams and flat surfaces. *International Journal for Numerical Methods in Engineering*, vol. 97, p. 683-706.

Gay Neto, A., Malta, E. R., Pimenta, P. M., 2015. Catenary riser sliding and rolling on seabed during induced lateral movement. *Marine Structures*, vol. 41, p. 223-243.

Gerstenberger, A., Wall, W. A., 2008. Enhancement of fixed-grid methods towards complex fluid-structure interaction applications. *International Journal for Numerical Methods in Fluids*, vol. 57, p.1227-1248.

Gerstenberger, A., Wall, W. A., 2010. An embedded Dirichlet formulation for 3D continua. *International Journal for Numerical Methods in Engineering*, vol. 82, p. 537-563.

Gomes, H. C., 2013. *Método dos Elementos Finitos com Fronteiras Imersas aplicado a Problemas de Dinâmica dos Fluidos e Interação Fluido-Estrutura*. PhD thesis, São Paulo, Universidade de São Paulo.

Gomes, H. C., Pimenta, P. M., 2015. Embedded interface with discontinuous Lagrange multipliers for fluid-structure interaction analysis. *International Journal for Computational Methods in Engineering Science and Mechanics*. vol. 16, p.98-111.

Küttler, U., Wall, W. A., 2008. Fixed-point fluid-structure interaction solvers with dynamic relaxation. *Computational Mechanics*, vol. 43, p. 61-72.

Pimenta, P. M., Campello, E. M. B., Wriggers, P., 2004. A fully nonlinear multiparameter shell model with thickness variation and a triangular shell finite element. *Computational Mechanics*, vol. 34, p. 181-193.

Tezduyar, T. E., Sathe, S., Senga, M., Aureli, L., 2005. Finite element modeling of fluidstructure interactions with spacetime and advanced mesh update techniques. *Proceedings og the 10th International Conference on Numerical Methods in Continuum Mechanics*.